Supporting Information

Silk-based Sealant with Tough Adhesion for Instant Hemostasis of Bleeding Tissues

Shumeng Bai,[a] Xueliang Zhang,[a] Pingqiang Cai,[b,c] Xiaowei Huang,[d] Yuqing Huang,[d] Rui Liu,[a] Mengya Zhang,[a] Jibin Song,[d] Xiaodong Chen*[b,c] and Huanghao Yang*[a,d]

[a] College of Biological Science and Engineering, Fuzhou University, Fuzhou 350108, People's Republic of China
E-mail: hhyang@fzu.edu.cn

[b] Innovative Center for Flexible Devices (iFLEX), School of Materials Science & Engineering, Nanyang Technological University, 50 Nanyang Avenue, Singapore 639798, Singapore
E-mail: chenxd@ntu.edu.sg
Webpage: http://www.ntu.edu.sg/home/chenxd/

[c] Max Planck - NTU Joint Lab for Artificial Senses, Nanyang Technological University, 50 Nanyang Avenue, Singapore 639798, Singapore

[d] MOE Key Laboratory for Analytical Science of Food Safety and Biology, Fujian Provincial Key Laboratory of Analysis and Detection Technology for Food Safety, State Key Laboratory of Photocatalysis on Energy and Environment, College of Chemistry, Fuzhou University, Fuzhou 350108, People's Republic of China

Keywords: biomimetic sealants, aqueous co-assembly, instant hemostasis, wet adhesion, phenolic chemistry

Experimental Section

Materials: *Bombyx mori* cocoons were purchased from Tianyou Silk Co. Ltd. (GuangXi, China). Tannic acid (TA) was obtained from Sigma-Aldrich (St. Louis, MO, USA). Calcein-AM and propidium iodide (PI) were purchased from Beyotime Biotechnology (Beijing, China). Live/Dead *Bac*Light bacterial viability kit was purchased from Thermo Fisher Scientific. All other chemicals were used as received from manufacturer.

Preparation of SFT: Silk fibroin (SF) aqueous solution was prepared according to our previously described approach.[1] In brief, *Bombyx mori* cocoons were boiled in 0.02 M Na_2CO_3 aqueous solution to remove sericin proteins. The degummed silk cocoons were dissolved in 9.3 M LiBr solution for 6 h and then dialyzed to obtain the fresh silk fibroin solution with a concentration of 5 wt.%. TA was dissolved in distilled water with a concentration of 0.3 g mL^{-1}. Then the TA solution was added to the SF solution with different ratios. A macroscopic adhesive gel was immediately formed after mixing the two solutions.

Characterization of SFT: The bonding interactions in forming SFT were analyzed by ^{1}H-NMR spectroscopy (Bruker AVANCE III 500 MHz), XPS spectroscopy (Thermo Scientific ESCALAB 250), CD spectrometer (AVIV Model 410), and FTIR spectroscopy (Thermo fisher Nicolet 6700). Rheological studies were performed on a rheometer (TA Instrument AR2000). Tensile test was measured by a texture analyzer (TA Instrument TA.XT Plus). Toughness was determined from the area of stress/strain curve. Three repeated experiments were conducted. Elastic modulus was calculated from the slope of stress/strain curve in the range of 5-15% strain.[2]

Molecular simulation methods: The coordinate of SF protein crystal structure was obtained and modified from RCSB Protein Data Bank (PDB entry: 3UA0).[3] Geometry optimization of TA was performed by B3LYP method with 6-31G* basis set in Gaussian 09 package. The parameters were carried out in General Amber Force Field form by Antechamber tool. RESP method was applied to fit the charge of TA.[4] All simulations were performed with GROMACS 5.0.4 package with Amber 99SB-ILDN all-atoms force field in the NPT ensemble. 20 ns MD simulation was applied for each SF-TA group. The free VMD software was used to visualize simulation results. Temperature was maintained at 300K by applying the Nose-Hoover thermostat coupling. The cut-off switching function for non-bonded van der Waals interaction started at 1.2 nm and reached zero at 1.35 nm. Particle mesh Ewald summation was used to calculate the long-range electrostatic interactions with a cut-off distance of 1.2 nm for the separation of the direct and reciprocal space.[5] The bond lengths were constrained by linear constraint solver algorithm and periodic boundary conditions were applied in all simulations. SF and TA were dissolved in simple point charge water molecules. The system was neutralized by sodium and chloride ions. Simulations were carried out with a time step of 2 fs and data were saved every 4 ps.

Adhesion testing: *In vitro* lap shear test was performed according to the modified ASTM standard F2255-05 method.[6] Briefly, fresh porcine skin was cut into sections at 3 cm × 1 cm size and 2 mm thick and wetted before use. The SFT material was spread over an area of 1 cm × 1 cm on one side of each section. Subsequently, the two sections were brought in close contact with opposite direction overlaps. The porcine skin tissues with SFT were kept in a humid chamber for 20 min, and then these two sections were placed in the mechanical tester. The shear strength needed to detach the two sections was monitored by Instron 1185 with a 100 N load cell. *In vitro* peeling adhesion strength was measured with 180-degree peeling adhesion test.[7] Briefly, the SFT material was applied uniformly between two unidirectional porcine skin sections with one end open and kept in a humid chamber for 20 min, forming a bilayer with an edge crack. The free ends of two skin sections were attached to the machine grips. An Instron machine 1185 with a 100 N load cell was used to apply the continuous tension with a 180-degree peeling direction. *In vitro* wound closure test was performed by using the ASTM F2458-05 standard.[8] Briefly, wet porcine skin section was fixed onto two poly(methyl methacrylate) slides with 6 mm spaces between the slides. The skin section was separated in the middle to simulate the wound, and then the SFT material was administered onto the cut area to reconnect the skin section for 20 min. Adhesion strength was obtained at the point of tearing. Three repeated experiments were conducted for each adhesion test. Fresh porcine skin pieces were harvested according to the protocol approved by the Institutional Animal Care and Use Committee of Fuzhou University. All experimental animal procedures were in agreement with the guide for the care and use of laboratory animals (Ministry of Science and Technology of China, 2006).

Clotting time assay: Clotting time test was performed according to a literature protocol.[9] Briefly, a volume of citrated blood was collected into an Eppendorf tube. 0.1 M calcium chloride was added in the tube and mixed with blood for 10 s. Then, 50 µL of mixture was deposited into sequential wells. At predetermined time intervals, each well was washed with saline solution. The liquid was immediately removed. The clotting time was marked in the well to form a uniform clot. For testing SFT, the SFT hydrogels were injected into sequential wells before the test, ensuring the entire bottom coated with SFT. Then, blood was mixed with 0.1 M calcium chloride and deposited into wells to measure clotting times. Three repeated experiments were conducted. Citrated blood was harvested from a male Wistar rat (200 to 250 g) according to the protocol approved by the Institutional Animal Care and Use Committee of Fuzhou University. All experimental animal procedures

were in agreement with the guide for the care and use of laboratory animals (Ministry of Science and Technology of China, 2006).

Antibacterial Measurement: The antibacterial activity of the SFT material was evaluated by using *S. aureus* (Gram-positive) bacteria as the representative model according to a literature procedure.[10] Briefly, *S. aureus* (1×10^6 CFU mL^{-1}) bacterial suspension was incubated with SFT material for 6 h at 37 °C, and their optical density at 600 nm (OD600) was tested. Representative of three experiments. Error bars show SD. Plating method was used to evaluate the antibacterial activity. The *S. aureus* bacterial suspension after treatment with SFT was spread on the solid medium and cultured to measure the number of the bacterial colonies. The LIVE/DEAD bacterial viability assay was further performed to confirm the antibacterial ability. The cell morphologies of *S. aureus* were observed by using a scanning electron microscopy (Hitach S4800).

In vitro biocompatibility test: Briefly, human synovial fibroblast (HSF) cells were cultured in RPMI-1640 media with 10% fetal bovine serum at 37 °C in a 5% CO_2 incubator. The sterilized SFT material (20 mg) was washed with 1 × PBS and incubated with 1 mL DMEM at 37 °C for 24 h to gain the conditioned medium. HSF cells were seeded in a 96 well plate and then incubated with the conditioned medium for 24 h.[7,11] Cell viabilities were determined with a LIVE/DEAD fluorescence staining assay by using calcein-AM and propidium iodide (PI). The fluorescent images of the cells were performed using a confocal laser scanning microscope. Further, cell viabilities were determined by CCK-8 assay.

In vivo degradation studies and histology: Animal experiments were executed according to the protocol approved by the Institutional Animal Care and Use Committee of Fuzhou University. All experimental animal procedures were in agreement with the guide for the care and use of laboratory animals (Ministry of Science and Technology of China, 2006). Briefly, a male Wistar rat (200 to 250 g) was anesthetized using ketamine and xylazine mixture. Then, a dorsal skin incision was created and subcutaneous pockets along the dorsomedial skin were generated. The SFT materials were lyophilized, weighted, and sterilized. Then the SFT materials were implanted in subcutaneous pockets. At days 15, 30, and 45 post-implantations, rats were euthanized, and the implanted materials were harvested and weighed. Skin tissues surrounding the materials were also collected for histological assessment.[8,12] Each group contained three rats.

Animal experiments for wound closure: A rat skin incision model was used to evaluate the *in vivo* wound closure effect of SFT. The male Wistar rat (200 to 250 g) was anesthetized using ketamine and xylazine mixture. A dorsal skin incision with 1 cm long and full-skin thickness depth was created. Then, the SFT material was immediately prepared in situ on the incision area. The cyanoacrylate was used as a control group. After 7 days, rats were euthanized and skin tissues at the incision site were obtained for histological assessment.[13] Each group contained three rats.

Animal experiments for liver hemostasis: A rat liver bleeding model was established to investigate the *in vivo* hemostatic ability of SFT. The male Wistar rat (200 to 250 g) was anesthetized using ketamine and xylazine mixture. Then the liver was dissected, and the bleeding was induced using an 18G needle. Immediately, the SFT material was prepared in situ on the bleeding site. The hemostatic time was calculated until the equilibrium state of liver hemostasis was reached. The mass of blood was measured by using the filter paper beneath the liver.[6,14] The cyanoacrylate was used as a control group. Each group contained three rats.

Animal experiments for heart hemostasis: A rat heart bleeding model was established to investigate the *in vivo* hemostatic ability of SFT. The male Wistar rat (200 to 250 g) was anesthetized using ketamine and xylazine mixture. The heart was exposed through a left thoracotomy and the bleeding was induced using a 23G needle. Then, the SFT material was immediately applied on the bleeding site of the beating heart and the hemostatic time was measured.[7,15] Each group contained three rats.

Animal experiments for intestine leakage: A rat intestine incision model was used to verify the in vivo leakage sealing capacity of SFT. The male Wistar rat (200 to 250 g) was anesthetized using ketamine and xylazine mixture. A surgical incision (2-4 mm) was created in the small intestine and the leakage at the incision site was confirmed by injecting the test dye. Then, the SFT material was immediately applied on the incision area and the leakage was reassessed.[12] Each group contained three rats.

Supporting Figures

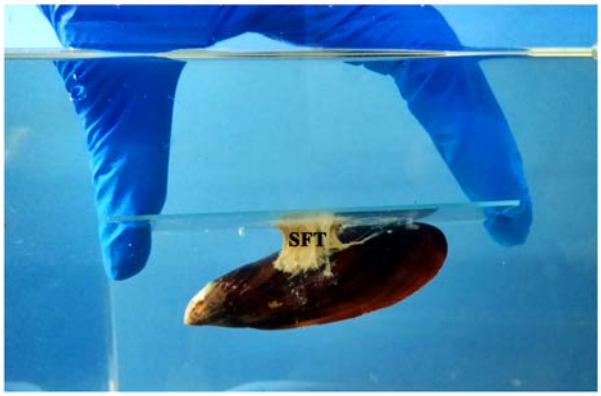

Fig. S1. Underwater adhesion behavior of SFT using a mussel as model.

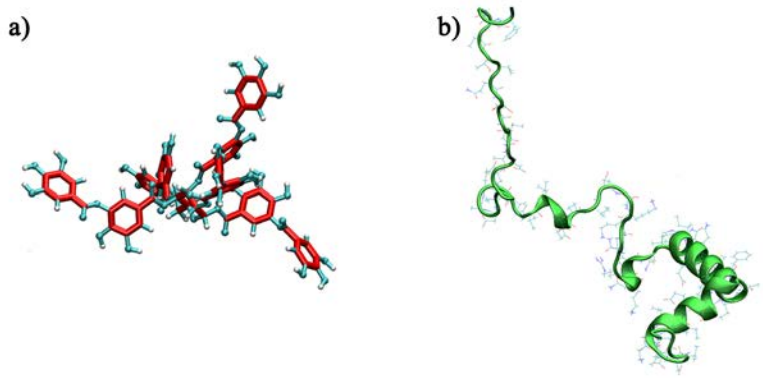

Fig. S2. a) The stick model of TA (containing multi-aromatic ring structures). Color code: red for carbon, cyan for oxygen and white for hydrogen. b) The three-dimension structures of the initial SF protein.

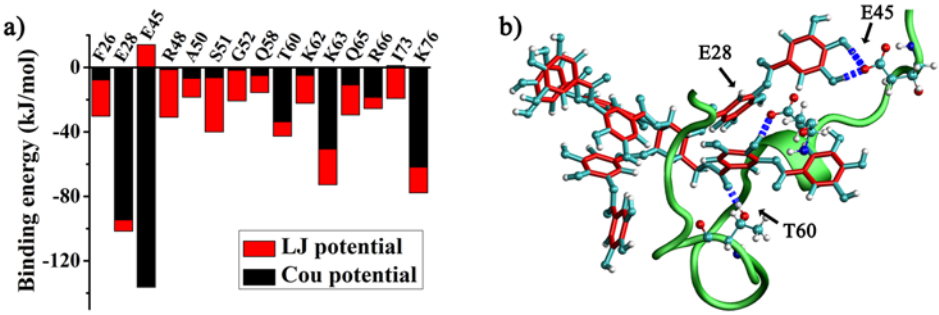

Fig. S3. a) The binding energies of TA and key amino acids of SF protein in the equilibrium simulation (the last 1 ns). Red: Lennard-Jones potential energy (LJ potential). Black: electrostatic potential energy (Cou potential). b) Simulation model of hydrogen bond interactions between TA and key amino acids of SF protein. Blue dotted lines: hydrogen bond.

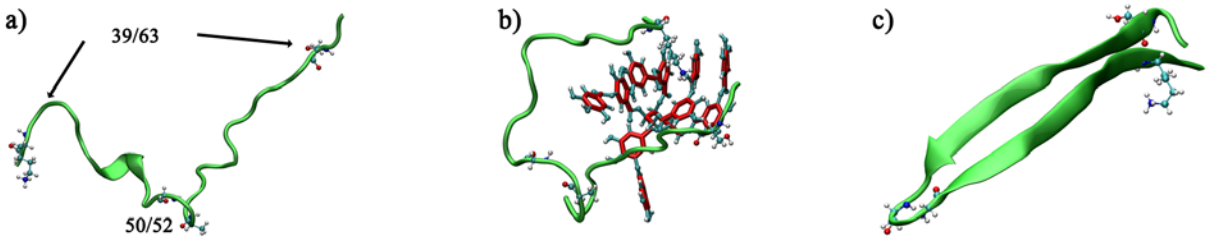

Fig. S4. TA induced and promoted the protein folding behaviors of SF. a) The initial conformation of amino acids in random coil SF protein. b) Amino acids in random coil SF protein were folded around the TA molecule to form similar β-sheet structure. c) The conformation of the corresponding amino acids in β-sheet SF protein.

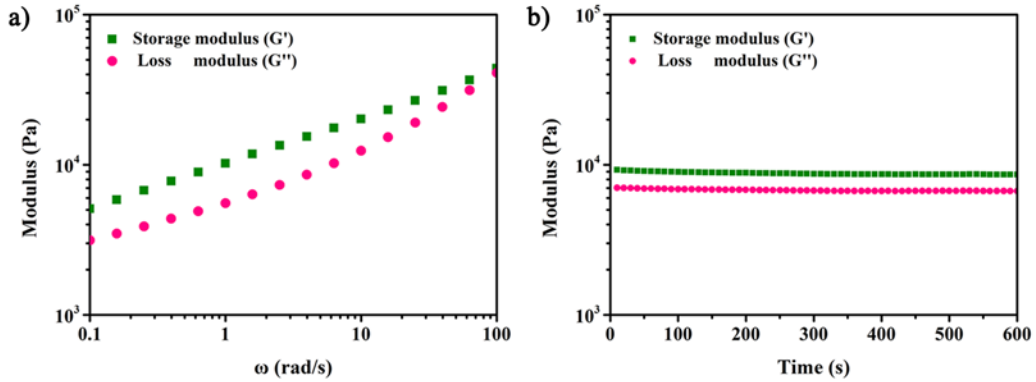

Fig. S5. Rheological analysis of SFT in a frequency sweep mode (a) and in a dynamic time sweep mode (b).

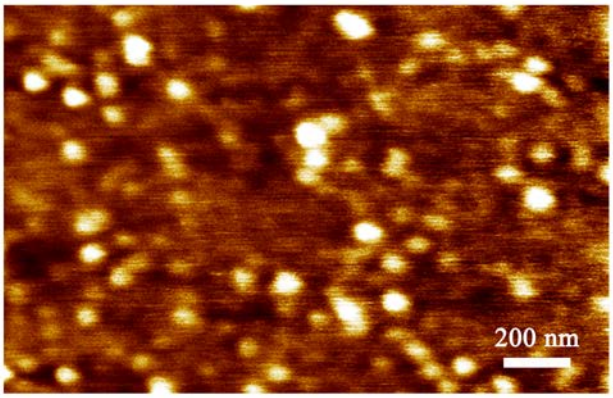

Fig. S6. AFM image of pure SF sample.

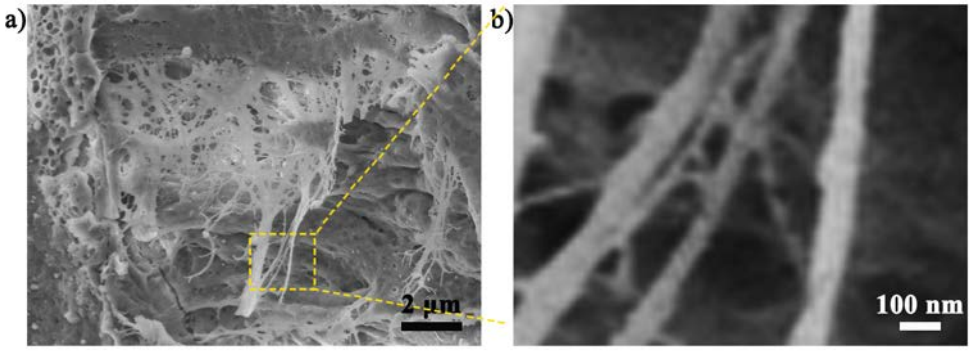

Fig. S7. SEM image of the SFT hydrogel.

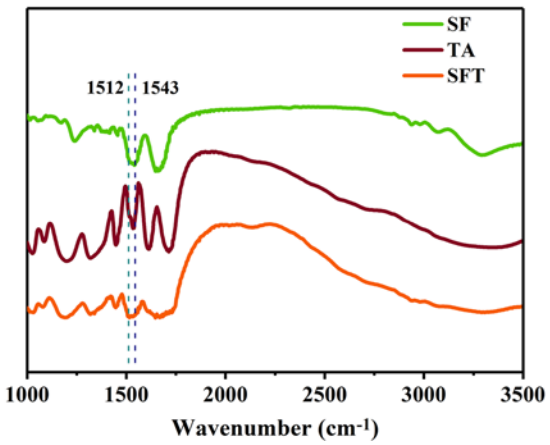

Fig. S8. The conformational analysis of SFT by FTIR spectroscopy. FTIR spectroscopy confirmed the structural changes of the SF protein.

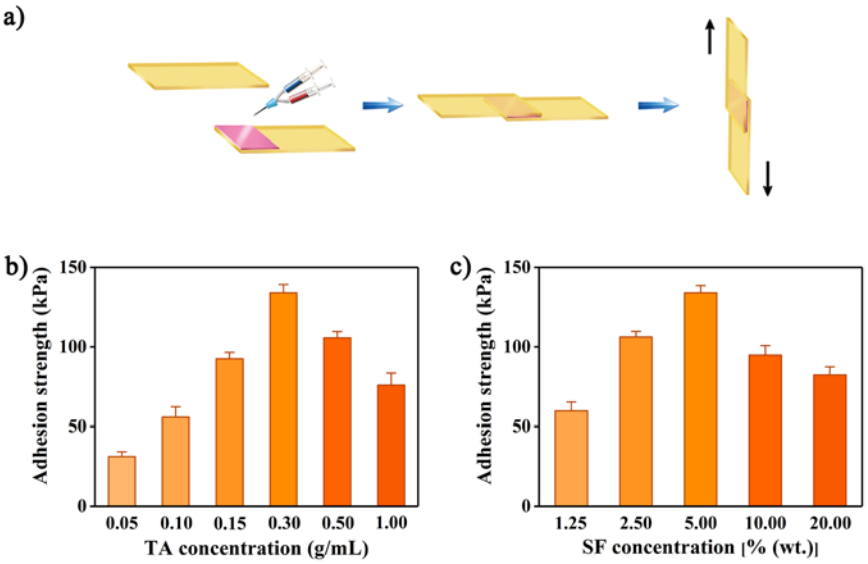

Fig. S9. a) Schematic of lap shear test to determine the adhesion strength of SFT using wet porcine skin as the substrate. b) Average shear adhesion strength of SFT produced by 5 wt.% SF solution with varying TA concentrations. c) Average shear adhesion strength of SFT produced by 0.3 g mL^{-1} TA solution with varying SF concentrations.

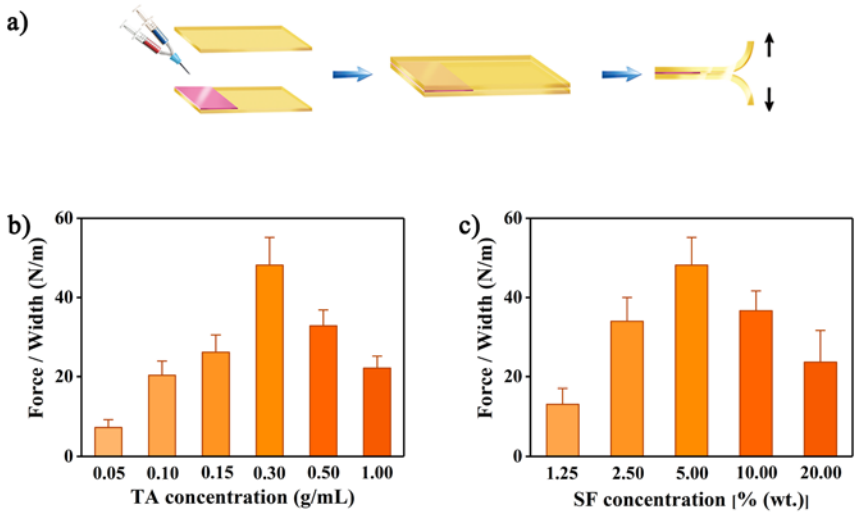

Fig. S10. a) Schematic of peeling adhesion test to determine the adhesion strength of SFT using wet porcine skin as the substrate. b) Average peeling adhesion strength of SFT produced by 5 wt.% SF solution with varying TA concentrations. c) Average peeling adhesion strength of SFT produced by 0.3 g mL^{-1} TA solution with varying SF concentrations. Error bars show SD.

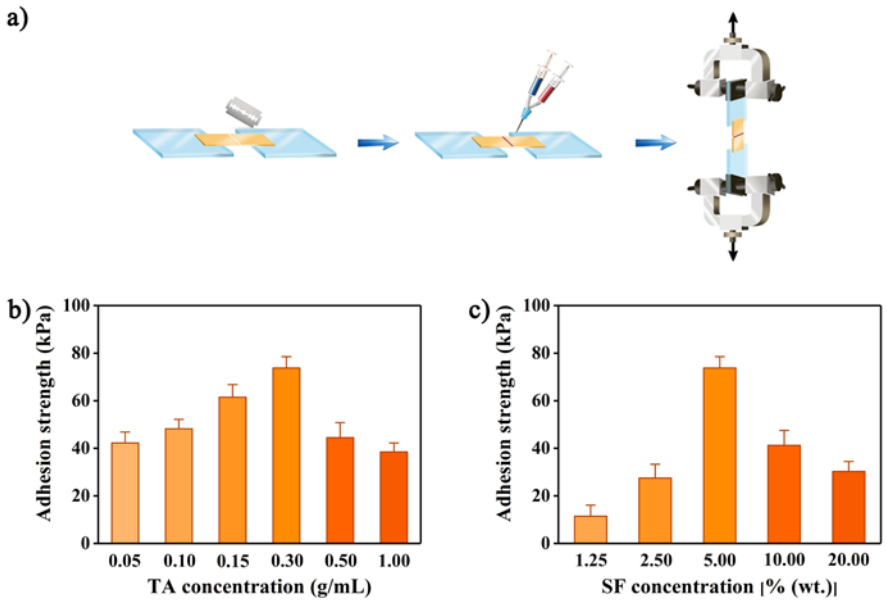

Fig. S11. a) Schematic of wound closure test to determine the adhesion strength of SFT using wet porcine skin as the substrate. b) Average sealing adhesion strength of SFT produced by 5 wt.% SF solution with varying TA concentrations. c) Average sealing adhesion strength of SFT produced by 0.3 g mL^{-1} TA solution with varying SF concentrations. Error bars show SD.

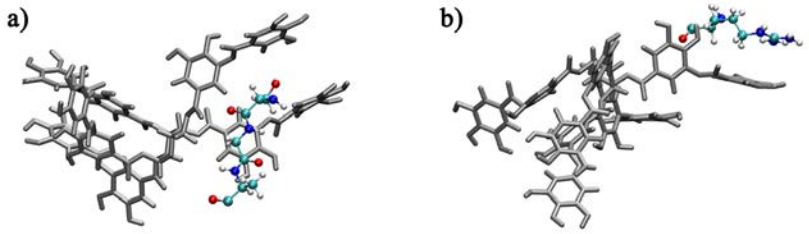

Fig. S12. π-π stacking models of van der Waals interactions between TA and amino acids, including π-π stacking of TA and peptide bond (a) and π-π stacking of TA and side-chain alkanes or rigid planar structures (b).

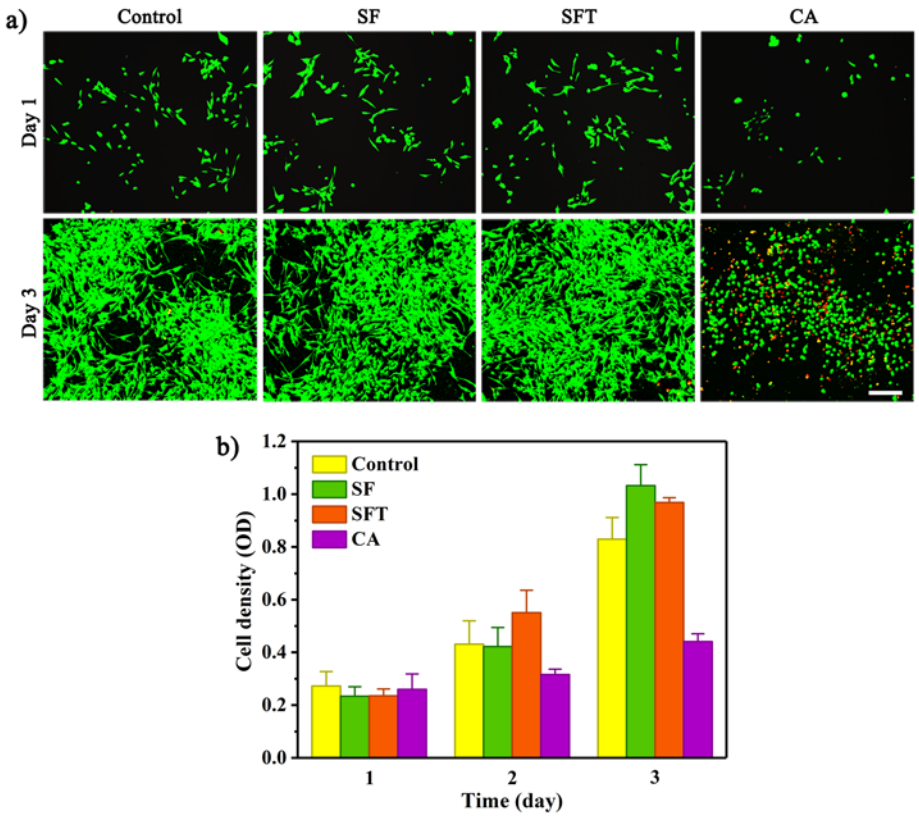

Fig. S13. a) Representative LIVE/DEAD images of viable (green, calcein-AM) and dead (red, PI) HSF cells incubated with SF conditioned medium, SFT conditioned medium, cyanoacrylate (CA) conditioned medium and without treatment (control). Scale bar: 200 µm. b) Corresponding cell viability study using HSF cells versus different culture times. Error bars show SD.

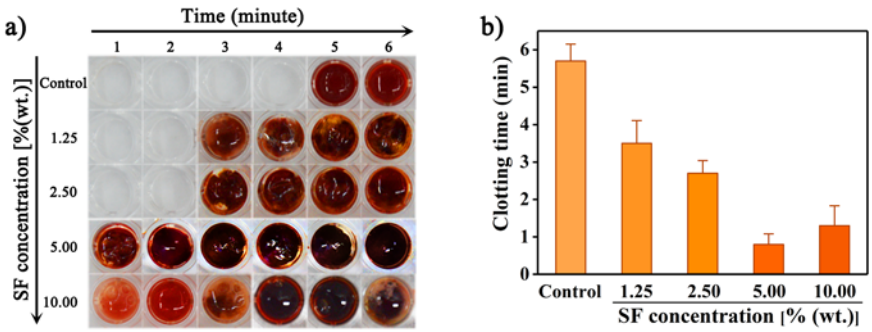

Fig. S14 a) Plate assay of blood clotting in contact with SFT produced by 0.3 g mL^{-1} TA solution with varying SF concentrations. b) Quantitative clotting time for SFT produced by 0.3 g mL^{-1} TA solution with varying SF concentrations. Error bars show SD.

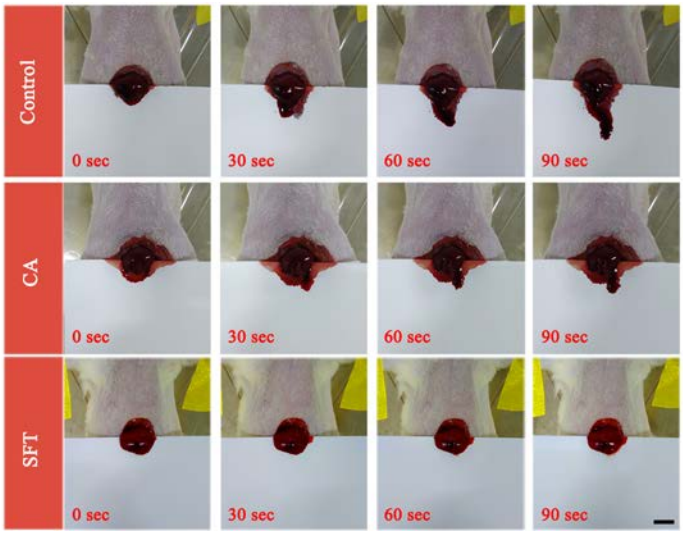

Fig. S15. Gross view of the bleeding livers treated with SFT, cyanoacrylate (CA), and without treatment (control) every 30 s in rat liver bleeding models. Scale bar: 1 cm.

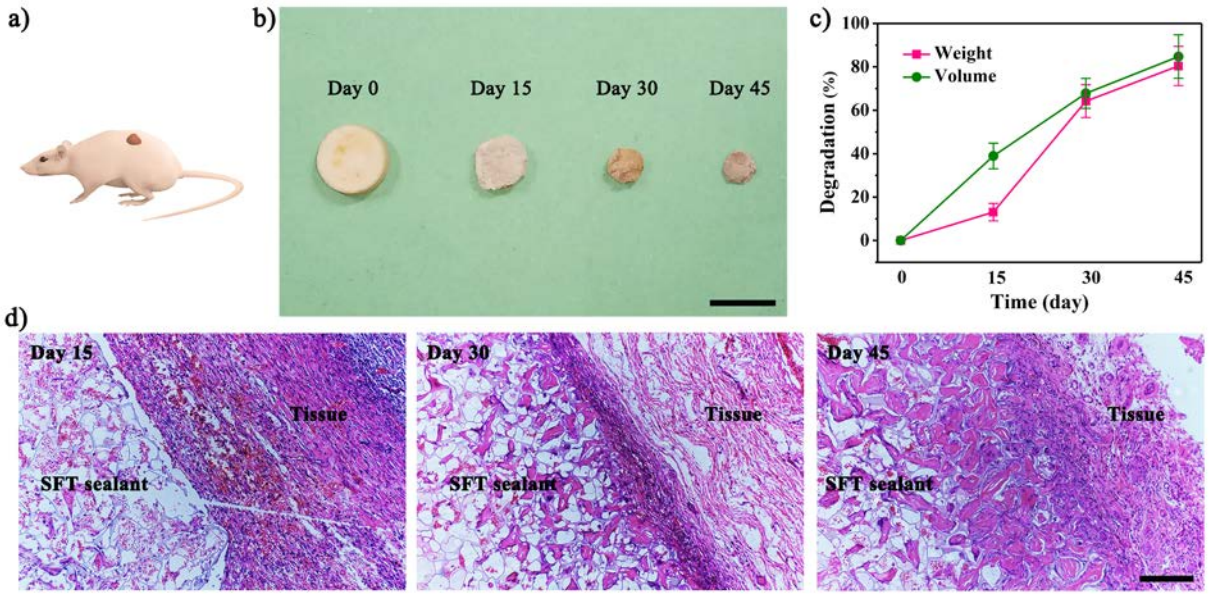

Fig. S16. a) Schematic of evaluation of the *in vivo* degradation of SFT using a rat subcutaneous model. b) Representative photograph images of SFT implants before and after subcutaneous implantation. Representative of three experiments. Scale bar: 1 cm. c) *In vivo* SFT degradation based on the weight and volume loss on days 0, 15, 30, and 45 after implantation. d) H&E staining of SFT with surrounding tissues after 15, 30, and 45 days of implantation. Representative of three experiments. Scale bar: 200 µm. Error bars show SD.

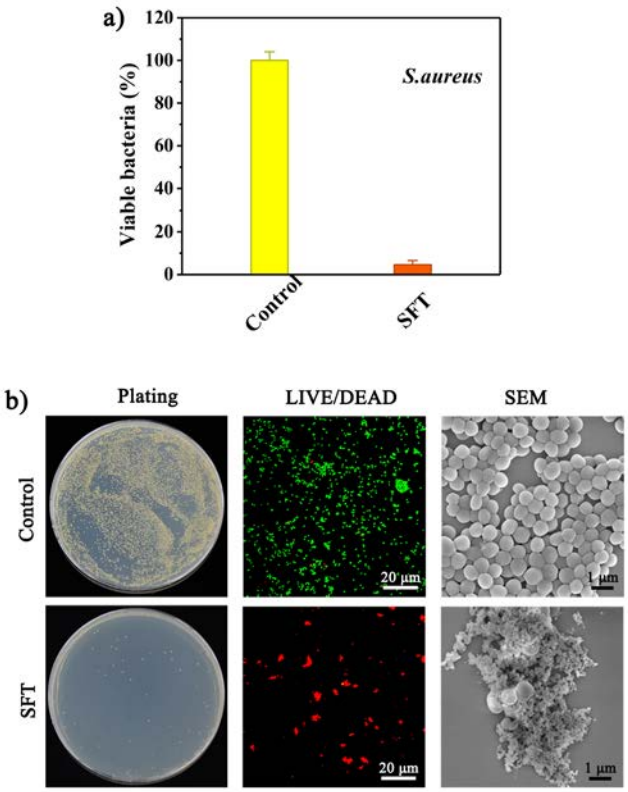

Fig. S17. a) Optical density at 600 nm of *S. aureus* bacterial suspensions after treatment with SFT and without treatment (control). b) Relative bacterial viabilities of *S. aureus* determined by a plating method, representative LIVE/DEAD images and typical morphology of *S. aureus* incubated with SFT and without treatment (control). Live bacteria with intact cell membranes exhibit green fluorescence, whereas bacteria with damaged membranes exhibited red fluorescence.

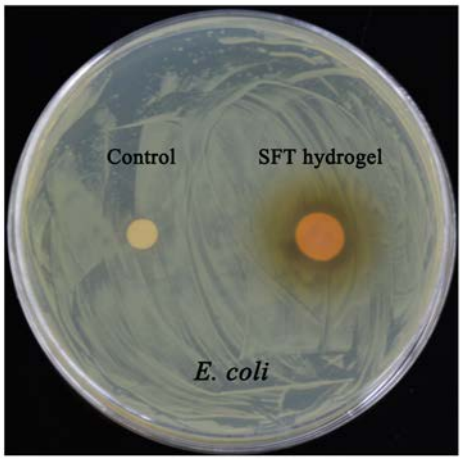

Fig. S18. Pictures of inhibition zones for bacterial from the sterilizing effectiveness test for *E. coli*.

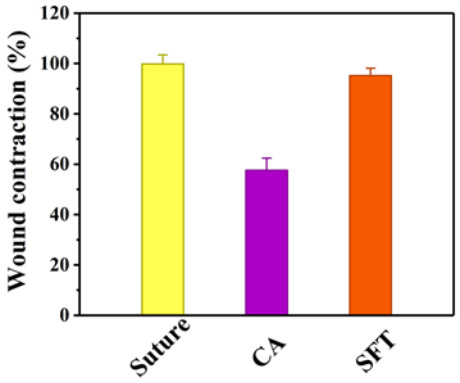

Fig. S19. Wound contraction for suturing treatment group, cyanoacrylate (CA) group, and SFT group on day 7 after surgery.

References

1 S. Bai, S. Liu, C. Zhang, W. Xu, Q. Lu, H. Han, D. L. Kaplan and H. Zhu, *Acta Biomaterialia*, 2013, **9**, 7806.

2 P. Lin, S. Ma, X. Wang and F. Zhou, *Adv. Mater.*, 2015, **27**, 2054.

3 Y. X. He, N. N. Zhang, W. F. Li, N. Jia, B. Y. Chen, K. Zhou, J. Zhang, Y. Chen and C. Z. Zhou, *J. Mol. Biol.*, 2012, **418**, 197.

4 J. Wang, W. Wang, P. A. Kollman and D. A. Case, *J. Mol. Graph. Model.*, 2006, **25**, 247.

5 T. Darden, D. York and L. Pedersen, *J. Chem. Phys.*, 1993, **98**, 10089.

6 R. Wang, J. Li, W. Chen, T. Xu, S. Yun, Z. Xu, Z. Xu, T. Sato, B. Chi and H. Xu, *Adv. Funct. Mater.*, 2017, **27**, 1604894.

7 J. Li, A. D. Celiz, J. Yang, Q. Yang, I. Wamala, W. Whyte, B. R. Seo, N. V. Vasilyev, J. J. Vlassak, Z. Suo and D. J. Mooney, *Science*, 2017, **357**, 378.

8 N. Annabi, D. Rana, E. S. Sani, R. Portillo-Lara, J. L. Gifford, M. M. Fares, S. M. Mithieux and A. S. Weiss, *Biomaterials*, 2017, **139**, 229.

9 A. K. Gaharwar, R. K. Avery, A. Assmann, A. Paul, G. H. Mckinley, A. Khademhosseini and B. D. Olsen, *ACS Nano*, 2014, **8**, 9833.

10 X. W. Huang, J. J. Wei, M. Y. Zhang, X. L. Zhang, X. F. Yin, C. H. Lu, J. B. Song, S. M. Bai and H. H. Yang, *ACS Appl. Mater. Interfaces*, 2018, **10**, 35495.

11 N. Ninan, A. Forget, V. P. Shastri, N. H. Voelcker and A. Blencowe, *ACS Appl. Mater. Interfaces*, 2016, **8**, 28511.

12 S. Hong, D. Pirovich, A. Kilcoyne, C. H. Huang, H. Lee and R. Weissleder, *Adv. Mater.*, 2016, **28**, 8675.

13 D. Lu, H. Wang, T. Li, Y. Li, X. Wang, P. Niu, H. Guo, S. Sun, X. Wang, X. Guan, H. Ma and Z. Lei, *Chem. Mater.*, 2017, **29**, 5493.

14 M. Shin, J. H. Ryu, J. P. Park, K. Kim, J. W. Yang and H. Lee, *Adv. Funct. Mater.*, 2015, **25**, 1270.

15 J. Shin, J. S. Lee, C. Lee, H. J. Park, K. Yang, Y. Jin, J. H. Ryu, K. S. Hong, S. H. Moon, H. M. Chung, H. S. Yang, S. H. Um, J. W. Oh, D. I. Kim, H. Lee and S. W. Cho, *Adv. Funct. Mater.*, 2015, **25**, 3814.

